

# Ratiometric imaging of catecholamine neurotransmitters with nanosensors

*Chen Ma<sup>a</sup>, Jennifer M. Mohr<sup>a</sup>, German Lauer<sup>c</sup>, Justus T. Metternich<sup>a,b</sup>, Krisztian Neutsch<sup>a</sup>, Tim Ziebarth<sup>c</sup>, Andreas Reiner<sup>c</sup>, Sebastian Kruss<sup>a, b \*</sup>*

<sup>a</sup> Department of Chemistry, Ruhr-University Bochum, Bochum, Germany

<sup>b</sup> Fraunhofer Institute for Microelectronic Circuits and Systems, Duisburg, Germany

<sup>c</sup> Department of Biology and Biotechnology, Ruhr-University Bochum, Bochum, Germany

**KEYWORDS:** Biosensors, near-infrared fluorescence, neurotransmitter, dopamine, carbon nanotubes, quantum defects

**ABSTRACT:** Neurotransmitters are important signaling molecules in the brain and relevant in many diseases. Measuring them with high spatial and temporal resolution in biological systems is challenging. Here, we develop a ratiometric fluorescent sensor/probe for catecholamine neurotransmitters based on near-infrared (NIR) semiconducting single wall carbon nanotubes (SWCNTs). Phenylboronic acid (PBA)-based quantum defects are incorporated into them to interact selectively with catechol moieties. These PBA-SWCNTs are further modified with polyethylene glycol phospholipids (PEG-PL) for biocompatibility. Catecholamines including

dopamine do not affect the intrinsic  $E_{11}$  fluorescence (990 nm) of these (PEG-PL-PBA-SWCNT) sensors. In contrast, the defect-related  $E_{11}^*$  emission (1130 nm) decreases by up to 35%. Furthermore, this dual-functionalization allows tuning selectivity by changing the charge of the PEG-polymer. These sensors are not taken up by cells, which is beneficial for extracellular imaging and they are functional in brain slices. In summary, we use dual-functionalization of SWCNTs to create a ratiometric biosensor for dopamine.

Detection of molecules is crucial for environmental monitoring, health, medicine, security, *etc.*<sup>1,2</sup> Common techniques include chromatography as well as electrochemical and optical microscopy and spectroscopy.<sup>3-5</sup> Optical biosensors have attracted increasing attention because of many advantages.<sup>6-8</sup> They enable fast readout in real-time with high spatiotemporal resolution. However, movements of the sample or variations of the illumination bias such measurements. To circumvent this issue self-calibrated approaches such as fluorescence lifetime (FLIM) imaging has been used.<sup>9,10</sup> Another approach is to use fluorescent sensors/probes with at least two emission features. One emission peak serves as reference and the second emission peak responds to the target analytes.<sup>11-14</sup> In the past, the advantages of ratiometric sensors have enabled *e.g.* improved calcium imaging but for most biomolecules ratiometric sensors do not exist.<sup>15</sup>

Such sensors are especially important to measure the fast chemical communication between cells for example *via* neurotransmitters. They are essential signaling molecules that transmit information between neurons in the brain. Disturbances in neurotransmitter concentration or regulation is linked to various diseases such as Parkinson's disease, schizophrenia, *etc.*<sup>16</sup> Monitoring and detecting the concentration of neurotransmitters could therefore provide insights into mechanisms or to diagnose/monitor these diseases. Over the past decades, electrochemical techniques and optical sensors including genetically encoded sensors have been developed to detect neurotransmitters.<sup>17,18</sup> Each technique has drawbacks as the low spatial resolution of electrochemical sensors or transfection of genetically encoded sensors or the lack of deep tissue penetration.<sup>19</sup>

Single wall carbon nanotubes (SWCNTs) are a material that could overcome these limitations because of their advantageous chemical and optical properties.<sup>20,21</sup> SWCNTs can be

conceptualized as rolled-up sheet of graphene. Semiconducting SWCNTs display fluorescence in the near-infrared (NIR) region, which overlaps with the tissue transparency window in which absorption and scattering are reduced. This makes them uniquely suited for biological applications and they therefore serve as versatile building blocks for biosensors.<sup>21–27</sup> However, due to the high hydrophobicity of SWCNTs, hydrophilic surface coatings are required to use them in aqueous environments. Surfactants or larger (bio)polymers that either form micelles around the SWCNTs or exhibit  $\pi$ - $\pi$  interactions are suitable for this purpose.<sup>28–30</sup> This non-covalent functionalization (corona) governs molecular interactions and photophysics.<sup>31–35</sup> For example, certain DNA modified SWCNTs such as (GT)<sub>10</sub>-coated SWCNTs are powerful dopamine sensors and were used to image dopamine release with high spatiotemporal resolution.<sup>33,36–39</sup> Similarly, SWCNTs modified with DNA aptamers are able to visualize serotonin release from blood platelets.<sup>40</sup> Additionally, SWCNTs-based biosensors have found applications in detecting proteins,<sup>41</sup> cancer markers,<sup>42,43</sup> reactive oxygen species (ROS),<sup>44–46</sup> and plant pathogens.<sup>47</sup> However, a disadvantage of non-covalently functionalized SWCNTs is the non-specific adsorption of biomolecules from biological fluids and their sensitivity towards ions.<sup>48,49</sup> Therefore, a robust surface coating is required to minimize non-specific adsorption. It has been shown that polyethylene glycol phospholipid (PEG-PL) coated SWCNTs display minimal non-specific adsorption.<sup>50,51</sup> Besides, PEG-PL-SWCNTs also show less interaction with cells and are used for extracellular tracking and microrheology.<sup>52–54</sup>

Apart from the non-covalent strategies, SWCNTs can be covalently functionalized. This includes guanine quantum defects<sup>55–57</sup> that reduce uptake by cells<sup>58</sup> and also serve as anchors for other recognition units.<sup>44</sup> In contrast,  $sp^3$  quantum defects in the  $sp^2$  lattice of SWCNTs generate a red-shifted emission peak ( $E_{11}^*$ ) and brighten their fluorescence.<sup>59–62</sup> They also serve as anchors to

conjugate biomolecules<sup>63,64</sup> and certain defects enable biosensing.<sup>65–67</sup> Examples include pH-sensitive quantum defects to study lysosomes and even *in vivo* monitoring.<sup>68</sup> Importantly, the number of quantum defects is on the order of 1-3 per SWCNT, which makes them well-defined recognition units and guarantees high sensitivity.<sup>69,70</sup> Quantum defects can also affect the sensing mechanism. For example, (GT)<sub>10</sub>-SWCNTs invert their optical response when they contain quantum defects.<sup>66</sup>

Biosensors require recognition units such as aptamers or antibodies. A well-established small recognition unit is boronic acids that interact with diols.<sup>71,72</sup> Nakashima *et al.* previously used boronic acids to decorate SWCNTs.<sup>73</sup> The emission of SWCNTs modified with phenylboronic acid (PBA) quantum defects shifted when saccharides bound, which was explained by electron withdrawal. However, this phenomenon occurred under basic conditions (pH ~13), which limits biological applications. Nevertheless, functionalization with quantum defects in combination with biocompatible coatings promises advances in biosensing.

Here, we describe a ratiometric sensor based on dual-functionalization of SWCNTs (Figure 1). It is based on the hypothesis that boronic acid quantum defects should bind diols including catecholamines. It is combined with non-covalent functionalization (PEG-PL) to block nonspecific adsorption, guarantee biocompatibility and tailor selectivity by changing the charge of the polymer. The quantum defect also creates a second fluorescence feature that is explored for ratiometric sensing. The biocompatibility of the nanosensor is then tested with cells and its functionality in brain slices to assess its potential.

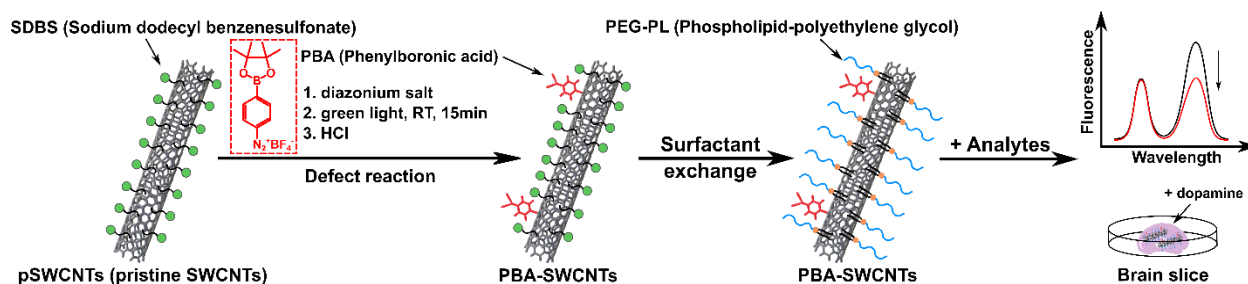


**Figure 1. Design of ratiometric catecholamine sensors with boronic acid quantum defects.** Single wall carbon nanotubes (SWCNTs) are modified with  $sp^3$  quantum defects that contain a phenyl boronic acid (PBA) moiety, which is known to bind diols. The non-biocompatible surfactant is then exchanged to PEG-PL or other (bio)polymers. This material emits the normal NIR fluorescence of SWCNTs and additionally a red-shifted defect-related fluorescence. This hybrid nanomaterial is explored as ratiometric sensor for catecholamine neurotransmitters such as dopamine.

To introduce PBA quantum defects into (6,5)-chirality enriched CoMoCAT SWCNTs, a diazonium salt derivative was synthesized from 4-aminophenylboronic acid pinacol ester. It was then added to sodium dodecyl benzenesulfonate (SDBS)-dispersed SWCNTs and irradiated with green light. After 15 min, hydrogen chloride (HCl) was added to the solution to release the boronic acid group for sensing. As a result, a peak at 1130 nm ( $E_{11}^*$ ) appeared in the NIR fluorescence spectrum (Figure 2a), and the ratio between the D and G modes of the Raman spectrum increased (Figure S1a), both indicating successful incorporation of quantum defects. Next, a surfactant exchange process<sup>74,75</sup> was performed to remove non-reacted diazonium salt and the surfactant to make PBA-SWCNTs biocompatible. PBA-SWCNTs were modified with PEG-PL to obtain PEG-PL-PBA-SWCNTs, which could be verified by a red-shift in absorption (Figure S1b) and NIR fluorescence spectra (Figure S1c,  $E_{11}$  peak shift from 980 nm to 991 nm).

To check the performance of PEG-PL-PBA-SWCNTs, 100  $\mu$ M dopamine was added. The  $E_{11}^*$  fluorescence significantly decreased by  $35\% \pm 2.05\%$  (SD) but  $E_{11}$  just slightly changed, and the ratio decreased by  $41\% \pm 2.42\%$  (SD) (Figure 2b). This is most likely caused by the specific interaction between PBA and the *ortho* hydroxy group of dopamine, which changes the emission

features of the quantum defects<sup>73</sup> and leads to a ratiometric readout ( $I_{E_{11}^*}/I_{E_{11}}$ ). Furthermore, the decrease in  $E_{11}^*$  fluorescence and  $I_{E_{11}^*}/I_{E_{11}}$  were concentration-dependent (Figure 2c). In addition, the binding affinity of PBA was tested. Both ascorbic acid and epinephrine also contain diol features and showed a similar behavior (Figure 2d) in a concentration-dependent manner (Figure S2). In contrast, the fluorescence of PEG-PL modified pristine SWCNTs (PEG-PL-pSWCNTs) did not change significantly in response to these analytes (Figure S3). Only at the highest tested concentration (100  $\mu$ M) the fluorescence of PEG-PL-pSWCNTs decreased but to a much smaller extent and we attribute this effect to non-specific interactions or dopamine polymerization. In contrast to the strong response of PEG-PL-PBA-SWCNTs to catecholamine neurotransmitters, other potentially interfering molecules with only one hydroxy group or hydroxy groups in *para* positions did not change the fluorescence (Figure 2e). Together, all these results demonstrate the selectivity of PEG-PL-PBA-SWCNTs for molecules with (*ortho*) diol groups.

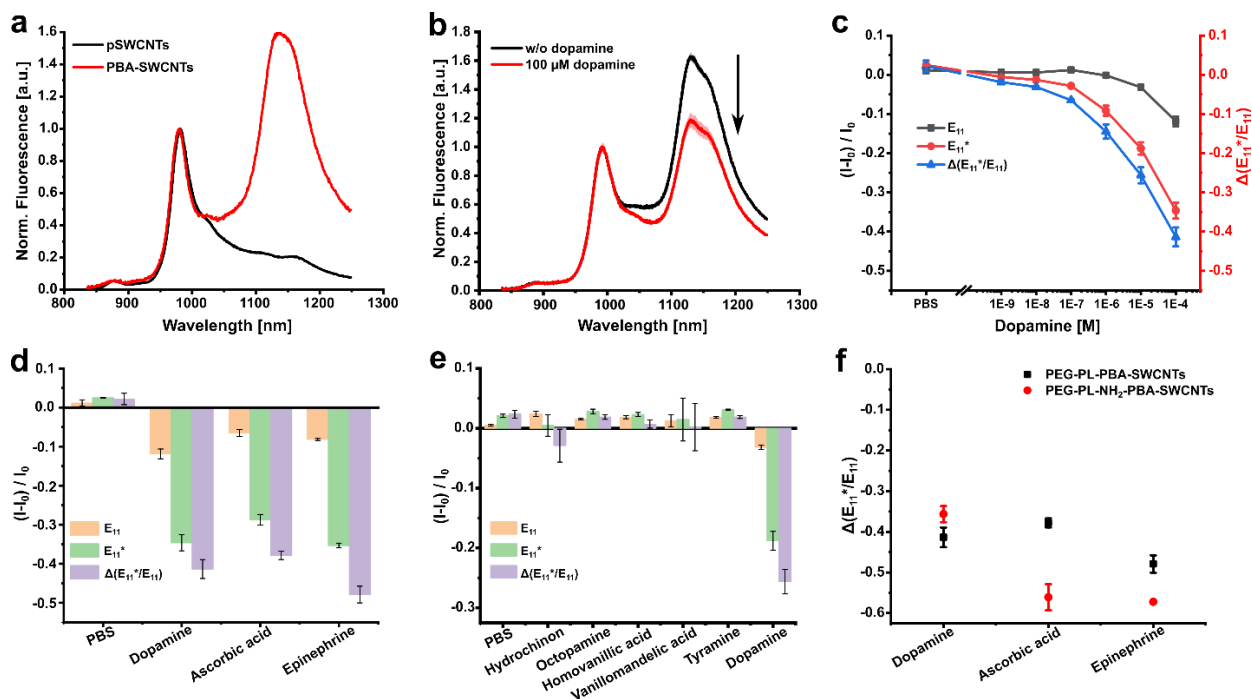


**Figure 2. Ratiometric NIR fluorescence sensing of catecholamines.** (a) Normalized NIR fluorescence spectra of (6,5)-SWCNTs before and after PBA quantum defect incorporation. (b) Normalized fluorescence response of PEG-PL-PBA-SWCNTs to 100  $\mu\text{M}$  dopamine in PBS (mean  $\pm$  SD,  $n = 3$ ). (c) Dose-response curve of PEG-PL-PBA-SWCNTs for dopamine (mean  $\pm$  SD,  $n = 3$ ). (d) Relative fluorescence intensity changes after PBS, dopamine, ascorbic acid and epinephrine addition in PBS (mean  $\pm$  SD,  $n = 3$ ). (e) Selectivity of PEG-PL-PBA-SWCNTs for dopamine compared to different related compounds (10  $\mu\text{M}$ ). (Mean  $\pm$  SD,  $n = 3$ ). (f) Impact of surface charge on selectivity for PEG-PL-NH<sub>2</sub>-PBA-SWCNTs and PEG-PL-PBA-SWCNTs (mean  $\pm$  SD,  $n = 3$ ).

DNA-coated SWCNTs e.g. (GT)<sub>10</sub>-SWCNTs or (GT)<sub>15</sub>-SWCNTs have been used previously as high affinity sensors to detect dopamine release. These sensors also respond to ascorbic acid,<sup>19,38,76</sup> making it challenging to distinguish it from dopamine. In our dual-functionalization approach, we have the additional opportunity to modify the non-covalent coating without compromising the recognition unit (PBA). We hypothesized that the charge of the PEG polymer headgroup would have an impact on selectivity and tested PEG-PL-NH<sub>2</sub> (PEG-PL-NH<sub>2</sub>-PBA-SWCNTs). Addition of the analytes decreased again the E<sub>11</sub><sup>\*</sup> fluorescence (Figure S4) and all three analytes caused concentration-dependent responses. When dopamine was added, the  $\Delta\left(\frac{I_{E_{11}^*}}{I_{E_{11}}}\right)$  of PEG-PL-PBA-SWCNTs decreased by 41%  $\pm$  2.42% (SD) and PEG-PL-NH<sub>2</sub>-PBA-SWCNTs by 35%  $\pm$  1.97%

(SD). For ascorbic acid PEG-PL-NH<sub>2</sub>-PBA-SWCNTs decreased 18% more than PEG-PL-PBA-SWCNTs. For epinephrine, the ratio decreased by 48% ± 2.14% (SD) for PEG-PL-PBA-SWCNTs versus 57% ± 0.30% (SD) for PEG-PL-NH<sub>2</sub>-PBA (Figure 2f). Therefore, PEG-PL-NH<sub>2</sub>-PBA-SWCNTs responded differently to dopamine and ascorbic acid, compared to the PEG-PL-PBA-SWCNTs, which showed similar responses to dopamine and ascorbic acid. A possible explanation is the additional positive charge that attracts negatively charged ascorbic acid and repels positively charged dopamine. Even though these results (roughly 2 fold increase in selectivity for dopamine versus ascorbic acid) are not yet demonstrating very high selectivity of ascorbic acid over dopamine (or vice versa) they indicate that the dual-functionalization approach has the potential to tailor selectivity.

DNA-SWCNTs are known to interact strongly with cells and are taken up by them, which is wanted for intracellular delivery. For many other applications this poses a challenge and affects the cells. In contrast, it is known that PEG-PL-SWCNTs show minimal nonspecific interaction with cells and are therefore commonly used for extracellular tracking.<sup>53,77</sup> To investigate the uptake of SWCNTs with different surface coatings (DNA and PEG-PL) by cells and the effect of PBA, HeLa cells were exposed to DNA-pSWCNTs, PEG-PL-pSWCNTs, and PEG-PL-PBA-SWCNTs. As expected, we observed a higher NIR fluorescence signal in cells incubated with (GT)<sub>10</sub>-pSWCNTs (Figure 3a). However, many SWCNTs can also be seen in the background, which is due to the interaction between (GT)<sub>10</sub>-SWCNTs and the glass substrate. Cells incubated with PEG-PL-pSWCNTs (Figure 3b) and PEG-PL-PBA-SWCNTs (Figure 3c) both showed a relatively low NIR fluorescence signal inside the cells and no adsorption of SWCNTs on glass was observed. (GT)<sub>10</sub>-SWCNTs showed the highest fluorescence inside cells (Figure 3d). No significant difference between PEG-PL-pSWCNTs and PBA-SWCNTs was observed, which makes sense

given the expected low number of (PBA) quantum defects.<sup>70</sup> These results indicate that PEG-PL coated PBA-SWCNTs are not effectively taken up by cells and remain mostly extracellular. This renders them suitable to detect secreted molecules and to perform extracellular imaging and tracking. Additionally, covalent functionalization with PBA had no effect on cellular uptake by PEG-PL-SWCNTs.

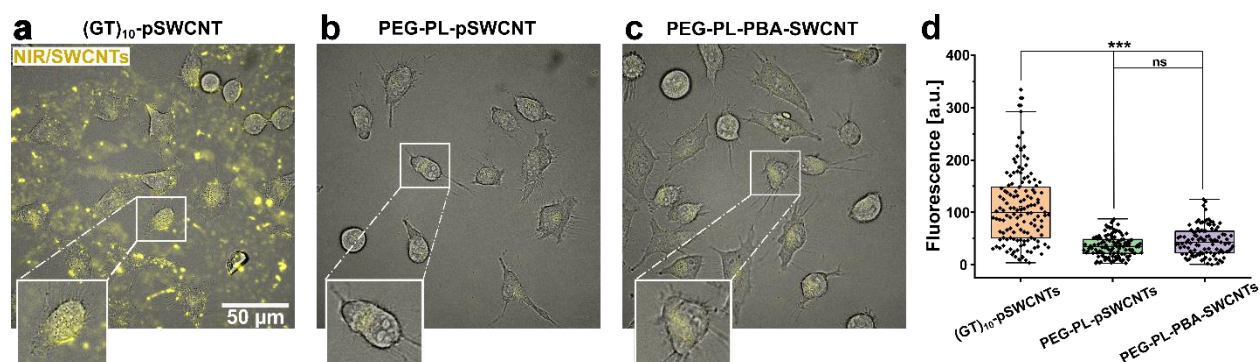


**Figure 3. PEG-PL coated catecholamine sensors show less interactions with cells.** Merged bright field (gray) and NIR fluorescence (yellow) images of HeLa cells incubated with (a) 0.4 nM (GT)<sub>10</sub>-SWCNTs, (b) 2 nM PEG-PL-pSWCNTs and (c) 2 nM PEG-PL-PBA-SWCNTs and magnified images of single cells (insert). (d) NIR fluorescence signal colocalization with HeLa cells shows less physisorption/uptake for PEG-PL-PBA-SWCNTs ( $N = 133, 118$  and  $105$  cells respectively) compared to DNA-coated SWCNTs. Two-sample test: \*\*\* $p < 0.001$ , ns = not significant.

Finally, we tested if PEG-PL-PBA-SWCNTs diffuse into brain slices and their functionality by exogenous application of dopamine. For this purpose, mouse brain slices were incubated with nanosensors (3 nM) for 15 min and subsequently transferred to a glass-bottom petri dish and rinsed twice to remove SWCNTs that did not diffuse into the tissue. They distributed relatively homogeneously within the slice (Figure 4a) matching the tissue architecture and freely accessible extracellular space. Then, time-dependent fluorescence images were recorded with a long-pass filter to detect the E<sub>11</sub>\* fluorescence (>1050 nm). During recording, 100 μM dopamine was added to the brain slice to examine the responsiveness of PEG-PL-PBA-SWCNTs. Before adding dopamine (*i.e.* in the first 300 s) and in control measurements without adding dopamine (900 s) the fluorescence intensity showed only a minor decrease most likely due to drift of the brain slice.

After dopamine addition fluorescence intensity decreased as expected (Figure 4b and S5b, Video M1). This behavior can also be seen on the single SWCNT level (Figure 4c). Single SWCNTs exhibited slightly different behaviors, with some showing an immediate and others a delayed decrease in fluorescence intensity, which might be due to differences in dopamine diffusion through the slice and the different positions of the SWCNTs inside it. However, all these results illustrate the functionality of PEG-PL-PBA-SWCNTs to detect dopamine in such a complex biological environment.

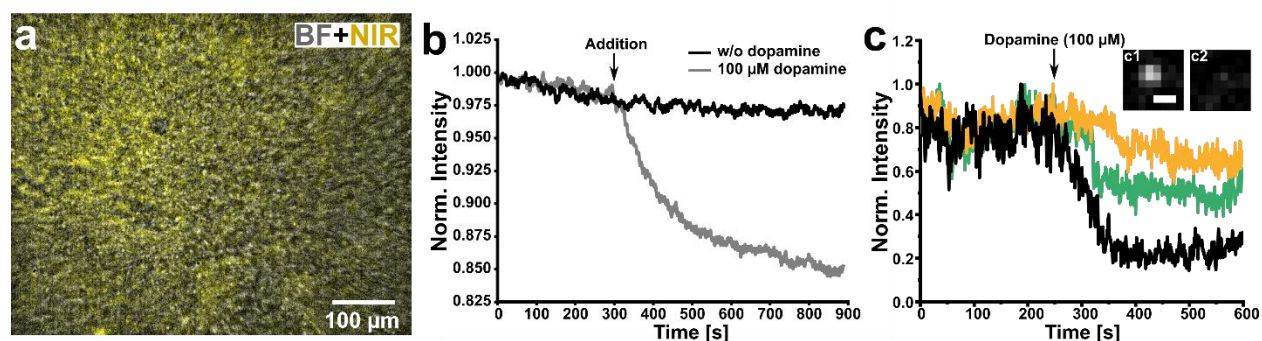


**Figure 4. Dopamine imaging with PEG-PL-PBA-SWCNTs in organotypic cortico-hippocampal brain slices.** (a) Merge of bright-field (gray) and NIR (yellow, >1050 nm) image of a brain slice. (b) Normalized overall NIR fluorescence intensity trace over 15 min. Dopamine was added at  $t = 300$  s. (c) Fluorescence traces of three single nanosensors inside the brain tissue. Dopamine was added at  $t = 240$  s. Image (c1, c2) of a single SWCNT before and after addition of dopamine (black trace in c). Scale bar = 1  $\mu$ m.

Ratiometric sensors provide technical advantages that enable novel and more complex experiments or more sensitive data analysis. SWCNT-based sensors have been used so far for many biomedical applications.<sup>21</sup> Previously, it was shown that one can combine SWCNTs of different chirality to create a ratiometric readout.<sup>76,78,79</sup> However, the ratiometric fluorescence readout was not encoded in single SWCNTs but different populations. The ratiometric response encoded in a single nanosensor is especially important in single-SWCNT imaging such as tracking of SWCNTs in extracellular space<sup>53,54</sup> or when they are immobilized on surfaces and high-resolution imaging of sensor responses is performed.<sup>80</sup> This design is therefore only possible by creating a second emission feature by the quantum defect. Another advantage is the dual-functionalization, which

opens chemical design opportunities to improve sensitivity and selectivity. In our case we used it to create by physisorption on the one side a non-responsive fluorescent signal and a surface chemistry that prevents uptake by cells. On the other side, we used the quantum defects as selective recognition unit for catecholamines. The possibility to tune sensor properties on different levels can be used for a broad range of existing sensors to push their performance. More robust fluorescence imaging is also possible by NIR FLIM as shown by us before.<sup>9</sup> However, such approaches are demanding optical setups capable of time correlated single photon counting (TCSPC), while ratiometric imaging can be performed in any wild field fluorescence microscope. Therefore, the intrinsic ratiometric sensor design presented here provides many opportunities for further developments including an extended chemical design space and promises higher performance in biomedical imaging.

In summary, we developed a ratiometric NIR fluorescent nanosensor by leveraging the dual-functionalization of SWCNTs. Technically, non-covalent modification of the SWCNT surface was combined with covalent functionalization (quantum defects) of SWCNTs. The boronic acid quantum defects create selectivity for catecholamines including dopamine while the polymer coating reduces non-specific interactions with cells. The second function of the quantum defects is a second fluorescence emission feature, which enables ratiometric sensing and imaging schemes. These parameters are important for experiments in complex biological systems such as mouse brain slices. Therefore, the approach pushes the limits of sensing and provides conceptual advances to optimize sensitivity, selectivity, and biocompatibility of nanosensors.

## ASSOCIATED CONTENT

**Supporting Information.** The Supporting Information is available free of charge via the Internet at <http://pubs.acs.org>. Details of materials and methods, additional spectra, videos, calibration curves, bright field images of a brain slice (PDF).

## AUTHOR INFORMATION

### Corresponding Author

\* Sebastian Kruss, Email: [sebastian.kruss@rub.de](mailto:sebastian.kruss@rub.de).

### Notes

The authors declare no competing financial interest.

## ACKNOWLEDGMENT

Funded by the Deutsche Forschungsgemeinschaft (DFG, German Research Foundation) under Germany's Excellence Strategy – EXC 2033 – 390677874 – RESOLV. This work is supported by the „Center for Solvation Science ZEMOS funded by the German Federal Ministry of Education and Research BMBF and by the Ministry of Culture and Research of Nord Rhine- Westphalia. We thank the DFG for funding within the Heisenberg program (S.K.). C.M. is financially supported by the China Scholarship Council. We thank the VW foundation for funding.

## REFERENCES

- (1) Howes, P. D.; Chandrawati, R.; Stevens, M. M. Colloidal Nanoparticles as Advanced Biological Sensors. *Science (1979)* **2014**, 346.
- (2) Lee, M. H.; Kim, J. S.; Sessler, J. L. Small Molecule-Based Ratiometric Fluorescence Probes for Cations, Anions, and Biomolecules. *Chem Soc Rev* **2015**, 44, 4185–4191.
- (3) Krämer, J.; Kang, R.; Grimm, L. M.; De Cola, L.; Picchetti, P.; Biedermann, F. Molecular Probes, Chemosensors, and Nanosensors for Optical Detection of Biorelevant Molecules and Ions in Aqueous Media and Biofluids. *Chem Rev* **2022**, 122, 3459–3636.

- (4) Klimuntowski, M.; Alam, M. M.; Singh, G.; Howlader, M. M. R. Electrochemical Sensing of Cannabinoids in Biofluids: A Noninvasive Tool for Drug Detection. *ACS Sens* **2020**, *5*, 620–636.
- (5) Hughes, C. C. Chemical Labeling Strategies for Small Molecule Natural Product Detection and Isolation. *Nat Prod Rep* **2021**, *38*, 1684–1705.
- (6) Yoo, S. M.; Lee, S. Y. Optical Biosensors for the Detection of Pathogenic Microorganisms. *Trends Biotechnol* **2016**, *34*, 7–25.
- (7) Askim, J. R.; Mahmoudi, M.; Suslick, K. S. Optical Sensor Arrays for Chemical Sensing: The Optoelectronic Nose. *Chem Soc Rev* **2013**, *42*, 8649.
- (8) Lei, Z.; Guo, B. 2D Material-Based Optical Biosensor: Status and Prospect. *Advanced Science* **2022**, *9*.
- (9) Sistemich, L.; Galonska, P.; Stegemann, J.; Ackermann, J.; Kruss, S. Near-Infrared Fluorescence Lifetime Imaging of Biomolecules with Carbon Nanotubes\*\*. *Angewandte Chemie International Edition* **2023**, *62*.
- (10) van der Linden, F. H.; Mahlandt, E. K.; Arts, J. J. G.; Beumer, J.; Puschhof, J.; de Man, S. M. A.; Chertkova, A. O.; Ponsioen, B.; Clevers, H.; van Buul, J. D.; Postma, M.; Gadella, T. W. J.; Goedhart, J. A Turquoise Fluorescence Lifetime-Based Biosensor for Quantitative Imaging of Intracellular Calcium. *Nat Commun* **2021**, *12*, 7159.
- (11) Huang, X.; Song, J.; Yung, B. C.; Huang, X.; Xiong, Y.; Chen, X. Ratiometric Optical Nanoprobes Enable Accurate Molecular Detection and Imaging. *Chem Soc Rev* **2018**, *47*, 2873–2920.
- (12) Chu, S.; Wang, H.; Ling, X.; Yu, S.; Yang, L.; Jiang, C. A Portable Smartphone Platform Using a Ratiometric Fluorescent Paper Strip for Visual Quantitative Sensing. *ACS Appl Mater Interfaces* **2020**, *12*, 12962–12971.
- (13) Wu, S.; Min, H.; Shi, W.; Cheng, P. Multicenter Metal–Organic Framework-Based Ratiometric Fluorescent Sensors. *Advanced Materials* **2020**, *32*.
- (14) Jia, R.; Tian, W.; Bai, H.; Zhang, J.; Wang, S.; Zhang, J. Amine-Responsive Cellulose-Based Ratiometric Fluorescent Materials for Real-Time and Visual Detection of Shrimp and Crab Freshness. *Nat Commun* **2019**, *10*, 795.
- (15) Thestrup, T.; Litzlbauer, J.; Bartholomäus, I.; Mues, M.; Russo, L.; Dana, H.; Kovalchuk, Y.; Liang, Y.; Kalamakis, G.; Laukat, Y.; Becker, S.; Witte, G.; Geiger, A.; Allen, T.; Rome, L. C.; Chen, T.-W.; Kim, D. S.; Garaschuk, O.; Griesinger, C.; Griesbeck, O. Optimized Ratiometric Calcium Sensors for Functional in Vivo Imaging of Neurons and T Lymphocytes. *Nat Methods* **2014**, *11*, 175–182.
- (16) Channer, B.; Matt, S. M.; Nickoloff-Bybel, E. A.; Pappa, V.; Agarwal, Y.; Wickman, J.; Gaskill, P. J. Dopamine, Immunity, and Disease. *Pharmacol Rev* **2023**, *75*, 62–158.

- (17) Patriarchi, T.; Cho, J. R.; Merten, K.; Howe, M. W.; Marley, A.; Xiong, W.-H.; Folk, R. W.; Broussard, G. J.; Liang, R.; Jang, M. J.; Zhong, H.; Dombeck, D.; von Zastrow, M.; Nimmerjahn, A.; Gradinaru, V.; Williams, J. T.; Tian, L. Ultrafast Neuronal Imaging of Dopamine Dynamics with Designed Genetically Encoded Sensors. *Science (1979)* **2018**, *360*.
- (18) Sun, F.; Zeng, J.; Jing, M.; Zhou, J.; Feng, J.; Owen, S. F.; Luo, Y.; Li, F.; Wang, H.; Yamaguchi, T.; Yong, Z.; Gao, Y.; Peng, W.; Wang, L.; Zhang, S.; Du, J.; Lin, D.; Xu, M.; Kreitzer, A. C.; Cui, G.; Li, Y. A Genetically Encoded Fluorescent Sensor Enables Rapid and Specific Detection of Dopamine in Flies, Fish, and Mice. *Cell* **2018**, *174*, 481-496.e19.
- (19) Dinarvand, M.; Elizarova, S.; Daniel, J.; Kruss, S. Imaging of Monoamine Neurotransmitters with Fluorescent Nanoscale Sensors. *ChempluSchem* **2020**, *85*, 1465–1480.
- (20) Bachilo, S. M.; Strano, M. S.; Kittrell, C.; Hauge, R. H.; Smalley, R. E.; Weisman, R. B. Structure-Assigned Optical Spectra of Single-Walled Carbon Nanotubes. *Science (1979)* **2002**, *298*, 2361–2366.
- (21) Ackermann, J.; Metternich, J. T.; Herbertz, S.; Kruss, S. Biosensing with Fluorescent Carbon Nanotubes. *Angewandte Chemie International Edition* **2022**, *61*.
- (22) Hendler-Neumark, A.; Bisker, G. Fluorescent Single-Walled Carbon Nanotubes for Protein Detection. *Sensors* **2019**, *19*, 5403.
- (23) Hong, G.; Diao, S.; Antaris, A. L.; Dai, H. Carbon Nanomaterials for Biological Imaging and Nanomedicinal Therapy. *Chem Rev* **2015**, *115*, 10816–10906.
- (24) Ackermann, J.; Stegemann, J.; Smola, T.; Reger, E.; Jung, S.; Schmitz, A.; Herbertz, S.; Erpenbeck, L.; Seidl, K.; Kruss, S. High Sensitivity Near-Infrared Imaging of Fluorescent Nanosensors. *Small* **2023**, 2206856.
- (25) Jeong, S.; Yang, D.; Beyene, A. G.; Del Bonis-O'Donnell, J. T.; Gest, A. M. M.; Navarro, N.; Sun, X.; Landry, M. P. High-Throughput Evolution of near-Infrared Serotonin Nanosensors. *Sci Adv* **2019**, *5*.
- (26) Safaee, M. M.; Gravely, M.; Roxbury, D. A Wearable Optical Microfibrous Biomaterial with Encapsulated Nanosensors Enables Wireless Monitoring of Oxidative Stress. *Adv Funct Mater* **2021**, *31*.
- (27) Williams, R. M.; Harvey, J. D.; Budhathoki-Uprety, J.; Heller, D. A. Glutathione-S-Transferase Fusion Protein Nanosensor. *Nano Lett* **2020**, *20*, 7287–7295.
- (28) Zheng, M.; Jagota, A.; Semke, E. D.; Diner, B. A.; Mclean, R. S.; Lustig, S. R.; Richardson, R. E.; Tassi, N. G. DNA-Assisted Dispersion and Separation of Carbon Nanotubes. *Nat Mater* **2003**, *2*, 338–342.
- (29) Williams, R. M.; Lee, C.; Heller, D. A. A Fluorescent Carbon Nanotube Sensor Detects the Metastatic Prostate Cancer Biomarker UPA. *ACS Sens* **2018**, *3*, 1838–1845.

- (30) López-Andarias, J.; Mejías, S. H.; Sakurai, T.; Matsuda, W.; Seki, S.; Feixas, F.; Osuna, S.; Aienza, C.; Martín, N.; Cortajarena, A. L. Toward Bioelectronic Nanomaterials: Photoconductivity in Protein–Porphyrin Hybrids Wrapped around SWCNT. *Adv Funct Mater* **2018**, *28*.
- (31) Polo, E.; Kruss, S. Impact of Redox-Active Molecules on the Fluorescence of Polymer-Wrapped Carbon Nanotubes. *The Journal of Physical Chemistry C* **2016**, *120*, 3061–3070.
- (32) Nißler, R.; Mann, F. A.; Chaturvedi, P.; Horlebein, J.; Meyer, D.; Vuković, L.; Kruss, S. Quantification of the Number of Adsorbed DNA Molecules on Single-Walled Carbon Nanotubes. *The Journal of Physical Chemistry C* **2019**, *123*, 4837–4847.
- (33) Kruss, S.; Salem, D. P.; Vuković, L.; Lima, B.; Vander Ende, E.; Boyden, E. S.; Strano, M. S. High-Resolution Imaging of Cellular Dopamine Efflux Using a Fluorescent Nanosensor Array. *Proceedings of the National Academy of Sciences* **2017**, *114*, 1789–1794.
- (34) Zhang, J.; Landry, M. P.; Barone, P. W.; Kim, J.-H.; Lin, S.; Ulissi, Z. W.; Lin, D.; Mu, B.; Boghossian, A. A.; Hilmer, A. J.; Rwei, A.; Hinckley, A. C.; Kruss, S.; Shandell, M. A.; Nair, N.; Blake, S.; Şen, F.; Şen, S.; Croy, R. G.; Li, D.; Yum, K.; Ahn, J.-H.; Jin, H.; Heller, D. A.; Essigmann, J. M.; Blankschtein, D.; Strano, M. S. Molecular Recognition Using Corona Phase Complexes Made of Synthetic Polymers Adsorbed on Carbon Nanotubes. *Nat Nanotechnol* **2013**, *8*, 959–968.
- (35) Ehrlich, R.; Hender-Neumark, A.; Wulf, V.; Amir, D.; Bisker, G. Optical Nanosensors for Real-Time Feedback on Insulin Secretion by B-Cells. *Small* **2021**, *17*, 2101660.
- (36) Kruss, S.; Landry, M. P.; Vander Ende, E.; Lima, B. M. A.; Reuel, N. F.; Zhang, J.; Nelson, J.; Mu, B.; Hilmer, A.; Strano, M. Neurotransmitter Detection Using Corona Phase Molecular Recognition on Fluorescent Single-Walled Carbon Nanotube Sensors. *J Am Chem Soc* **2014**, *136*, 713–724.
- (37) Mann, F.; Herrmann, N.; Meyer, D.; Kruss, S. Tuning Selectivity of Fluorescent Carbon Nanotube-Based Neurotransmitter Sensors. *Sensors* **2017**, *17*, 1521.
- (38) Elizarova, S.; Chouaib, A. A.; Shaib, A.; Hill, B.; Mann, F.; Brose, N.; Kruss, S.; Daniel, J. A. A Fluorescent Nanosensor Paint Detects Dopamine Release at Axonal Varicosities with High Spatiotemporal Resolution. *Proceedings of the National Academy of Sciences* **2022**, *119*, 2021.03.28.437019.
- (39) Beyene, A. G.; Delevich, K.; Del Bonis-O'Donnell, J. T.; Piekarski, D. J.; Lin, W. C.; Thomas, A. W.; Yang, S. J.; Kosillo, P.; Yang, D.; Prounis, G. S.; Wilbrecht, L.; Landry, M. P. Imaging Striatal Dopamine Release Using a Nongenetically Encoded near Infrared Fluorescent Catecholamine Nanosensor. *Sci Adv* **2019**, *5*.
- (40) Dinarvand, M.; Neubert, E.; Meyer, D.; Selvaggio, G.; Mann, F. A.; Erpenbeck, L.; Kruss, S. Near-Infrared Imaging of Serotonin Release from Cells with Fluorescent Nanosensors. *Nano Lett* **2019**, *19*, 6604–6611.

- (41) Bisker, G.; Dong, J.; Park, H. D.; Iverson, N. M.; Ahn, J.; Nelson, J. T.; Landry, M. P.; Kruss, S.; Strano, M. S. Protein-Targeted Corona Phase Molecular Recognition. *Nat Commun* **2016**, *7*, 10241.
- (42) Williams, R. M.; Lee, C.; Galassi, T. V.; Harvey, J. D.; Leicher, R.; Sirenko, M.; Dorso, M. A.; Shah, J.; Olvera, N.; Dao, F.; Levine, D. A.; Heller, D. A. Noninvasive Ovarian Cancer Biomarker Detection via an Optical Nanosensor Implant. *Sci Adv* **2018**, *4*.
- (43) Yaari, Z.; Yang, Y.; Apfelbaum, E.; Cupo, C.; Settle, A. H.; Cullen, Q.; Cai, W.; Roche, K. L.; Levine, D. A.; Fleisher, M.; Ramanathan, L.; Zheng, M.; Jagota, A.; Heller, D. A. A Perception-Based Nanosensor Platform to Detect Cancer Biomarkers. *Sci Adv* **2021**, *7*.
- (44) Metternich, J. T.; Wartmann, J. A. C.; Sistemich, L.; Nißler, R.; Herbertz, S.; Kruss, S. Near-Infrared Fluorescent Biosensors Based on Covalent DNA Anchors. *J Am Chem Soc* **2023**, *145*, 14776–14783.
- (45) Lew, T. T. S.; Koman, V. B.; Silmore, K. S.; Seo, J. S.; Gordiichuk, P.; Kwak, S.-Y.; Park, M.; Ang, M. C.-Y.; Khong, D. T.; Lee, M. A.; Chan-Park, M. B.; Chua, N.-H.; Strano, M. S. Real-Time Detection of Wound-Induced H<sub>2</sub>O<sub>2</sub> Signalling Waves in Plants with Optical Nanosensors. *Nat Plants* **2020**, *6*, 404–415.
- (46) Wu, H.; Nißler, R.; Morris, V.; Herrmann, N.; Hu, P.; Jeon, S.-J.; Kruss, S.; Giraldo, J. P. Monitoring Plant Health with Near-Infrared Fluorescent H<sub>2</sub>O<sub>2</sub> Nanosensors. *Nano Lett* **2020**, *20*, 2432–2442.
- (47) Nißler, R.; Müller, A. T.; Dohrman, F.; Kurth, L.; Li, H.; Cosio, E. G.; Flavel, B. S.; Giraldo, J. P.; Mithöfer, A.; Kruss, S. Detection and Imaging of the Plant Pathogen Response by Near-Infrared Fluorescent Polyphenol Sensors. *Angewandte Chemie International Edition* **2022**, *61*.
- (48) Pinals, R. L.; Yang, D.; Rosenberg, D. J.; Chaudhary, T.; Crothers, A. R.; Iavarone, A. T.; Hammel, M.; Landry, M. P. Quantitative Protein Corona Composition and Dynamics on Carbon Nanotubes in Biological Environments. *Angewandte Chemie International Edition* **2020**, *59*, 23668–23677.
- (49) Gillen, A. J.; Kupis-Rozmysłowicz, J.; Gigli, C.; Schuergers, N.; Boghossian, A. A. Xeno Nucleic Acid Nanosensors for Enhanced Stability Against Ion-Induced Perturbations. *J Phys Chem Lett* **2018**, *9*, 4336–4343.
- (50) Liu, Z.; Cai, W.; He, L.; Nakayama, N.; Chen, K.; Sun, X.; Chen, X.; Dai, H. In Vivo Biodistribution and Highly Efficient Tumour Targeting of Carbon Nanotubes in Mice. *Nat Nanotechnol* **2007**, *2*, 47–52.
- (51) Iverson, N. M.; Barone, P. W.; Shandell, M.; Trudel, L. J.; Sen, S.; Sen, F.; Ivanov, V.; Atolia, E.; Farias, E.; McNicholas, T. P.; Reuel, N.; Parry, N. M. A.; Wogan, G. N.; Strano, M. S. In Vivo Biosensing via Tissue-Localizable near-Infrared-Fluorescent Single-Walled Carbon Nanotubes. *Nat Nanotechnol* **2013**, *8*, 873–880.

- (52) Gao, Z.; Varela, J. A.; Groc, L.; Lounis, B.; Cognet, L. Toward the Suppression of Cellular Toxicity from Single-Walled Carbon Nanotubes. *Biomater Sci* **2016**, *4*, 230–244.
- (53) Godin, A. G.; Varela, J. A.; Gao, Z.; Danné, N.; Dupuis, J. P.; Lounis, B.; Groc, L.; Cognet, L. Single-Nanotube Tracking Reveals the Nanoscale Organization of the Extracellular Space in the Live Brain. *Nat Nanotechnol* **2017**, *12*, 238–243.
- (54) Soria, F. N.; Paviolo, C.; Doudnikoff, E.; Arotcarena, M.-L.; Lee, A.; Danné, N.; Mandal, A. K.; Gosset, P.; Dehay, B.; Groc, L.; Cognet, L.; Bezard, E. Synucleinopathy Alters Nanoscale Organization and Diffusion in the Brain Extracellular Space through Hyaluronan Remodeling. *Nat Commun* **2020**, *11*, 3440.
- (55) Zheng, Y.; Bachilo, S. M.; Weisman, R. B. Controlled Patterning of Carbon Nanotube Energy Levels by Covalent DNA Functionalization. *ACS Nano* **2019**, *13*, 8222–8228.
- (56) Zheng, Y.; Kim, Y.; Jones, A. C.; Olinger, G.; Bittner, E. R.; Bachilo, S. M.; Doorn, S. K.; Weisman, R. B.; Piryatinski, A.; Htoon, H. Quantum Light Emission from Coupled Defect States in DNA-Functionalized Carbon Nanotubes. *ACS Nano* **2021**, *15*, 10406–10414.
- (57) Lin, Z.; Beltrán, L. C.; De los Santos, Z. A.; Li, Y.; Adel, T.; Fagan, J. A.; Hight Walker, A. R.; Egelman, E. H.; Zheng, M. DNA-Guided Lattice Remodeling of Carbon Nanotubes. *Science (1979)* **2022**, *377*, 535–539.
- (58) Galonska, P.; Mohr, J. M.; Schrage, C. A.; Schnitzler, L.; Kruss, S. Guanine Quantum Defects in Carbon Nanotubes for Biosensing. *J Phys Chem Lett* **2023**, *14*, 3483–3490.
- (59) Piao, Y.; Meany, B.; Powell, L. R.; Valley, N.; Kwon, H.; Schatz, G. C.; Wang, Y. Brightening of Carbon Nanotube Photoluminescence through the Incorporation of Sp<sup>3</sup> Defects. *Nat Chem* **2013**, *5*, 840–845.
- (60) Zaumseil, J. Luminescent Defects in Single-Walled Carbon Nanotubes for Applications. *Adv Opt Mater* **2022**, *10*, 2101576.
- (61) Brozena, A. H.; Kim, M.; Powell, L. R.; Wang, Y. Controlling the Optical Properties of Carbon Nanotubes with Organic Colour-Centre Quantum Defects. *Nat Rev Chem* **2019**, *3*, 375–392.
- (62) Janas, D. Perfectly Imperfect: A Review of Chemical Tools for Exciton Engineering in Single-Walled Carbon Nanotubes. *Mater Horiz* **2020**, *7*, 2860–2881.
- (63) Mann, F. A.; Herrmann, N.; Opazo, F.; Kruss, S. Quantum Defects as a Toolbox for the Covalent Functionalization of Carbon Nanotubes with Peptides and Proteins. *Angewandte Chemie International Edition* **2020**, *59*, 17732–17738.
- (64) Mann, F. A.; Galonska, P.; Herrmann, N.; Kruss, S. Quantum Defects as Versatile Anchors for Carbon Nanotube Functionalization. *Nat Protoc* **2022**, *17*, 727–747.
- (65) Kim, M.; Chen, C.; Wang, P.; Mulvey, J. J.; Yang, Y.; Wun, C.; Antman-Passig, M.; Luo, H.-B.; Cho, S.; Long-Roche, K.; Ramanathan, L. V.; Jagota, A.; Zheng, M.; Wang, Y.; Heller, D. A. Detection of Ovarian Cancer via the Spectral Fingerprinting of Quantum-

- Defect-Modified Carbon Nanotubes in Serum by Machine Learning. *Nat Biomed Eng* **2022**, *6*, 267–275.
- (66) Spreinat, A.; Dohmen, M. M.; Lüttgens, J.; Herrmann, N.; Klepzig, L. F.; Nißler, R.; Weber, S.; Mann, F. A.; Lauth, J.; Kruss, S. Quantum Defects in Fluorescent Carbon Nanotubes for Sensing and Mechanistic Studies. *The Journal of Physical Chemistry C* **2021**, *125*, 18341–18351.
- (67) Kwon, H.; Kim, M.; Meany, B.; Piao, Y.; Powell, L. R.; Wang, Y. Optical Probing of Local pH and Temperature in Complex Fluids with Covalently Functionalized, Semiconducting Carbon Nanotubes. *The Journal of Physical Chemistry C* **2015**, *119*, 3733–3739.
- (68) Kim, M.; Chen, C.; Yaari, Z.; Frederiksen, R.; Randall, E.; Wollowitz, J.; Cupo, C.; Wu, X.; Shah, J.; Worroll, D.; Lagenbacher, R. E.; Goerzen, D.; Li, Y.-M.; An, H.; Wang, Y.; Heller, D. A. Nanosensor-Based Monitoring of Autophagy-Associated Lysosomal Acidification in Vivo. *Nat Chem Biol* **2023**, *19*, 1448–1457.
- (69) Sebastian, F. L.; Zorn, N. F.; Settele, S.; Lindenthal, S.; Berger, F. J.; Bendel, C.; Li, H.; Flavel, B. S.; Zaumseil, J. Absolute Quantification of Sp<sup>3</sup> Defects in Semiconducting Single-Wall Carbon Nanotubes by Raman Spectroscopy. *J Phys Chem Lett* **2022**, *13*, 3542–3548.
- (70) Ma, C.; Schrage, C. A.; Gretz, J.; Akhtar, A.; Sistemich, L.; Schnitzler, L.; Li, H.; Tschulik, K.; Flavel, B. S.; Kruss, S. Stochastic Formation of Quantum Defects in Carbon Nanotubes. *ACS Nano* **2023**, *17*, 15989–15998.
- (71) Bull, S. D.; Davidson, M. G.; van den Elsen, J. M. H.; Fossey, J. S.; Jenkins, A. T. A.; Jiang, Y.-B.; Kubo, Y.; Marken, F.; Sakurai, K.; Zhao, J.; James, T. D. Exploiting the Reversible Covalent Bonding of Boronic Acids: Recognition, Sensing, and Assembly. *Acc Chem Res* **2013**, *46*, 312–326.
- (72) Fang, G.; Wang, H.; Bian, Z.; Sun, J.; Liu, A.; Fang, H.; Liu, B.; Yao, Q.; Wu, Z. Recent Development of Boronic Acid-Based Fluorescent Sensors. *RSC Adv* **2018**, *8*, 29400–29427.
- (73) Shiraki, T.; Onitsuka, H.; Shiraishi, T.; Nakashima, N. Near Infrared Photoluminescence Modulation of Single-Walled Carbon Nanotubes Based on a Molecular Recognition Approach. *Chemical Communications* **2016**, *52*, 12972–12975.
- (74) Yang, Y.; Sharma, A.; Noetinger, G.; Zheng, M.; Jagota, A. Pathway-Dependent Structures of DNA-Wrapped Carbon Nanotubes: Direct Sonication vs Surfactant/DNA Exchange. *Journal of Physical Chemistry C* **2020**, *124*, 9045–9055.
- (75) Streit, J. K.; Fagan, J. A.; Zheng, M. A Low Energy Route to DNA-Wrapped Carbon Nanotubes via Replacement of Bile Salt Surfactants. *Anal Chem* **2017**, *89*, 10496–10503.
- (76) Nißler, R.; Kurth, L.; Li, H.; Spreinat, A.; Kuhlemann, I.; Flavel, B. S.; Kruss, S. Sensing with Chirality-Pure Near-Infrared Fluorescent Carbon Nanotubes. *Anal Chem* **2021**, *93*, 6446–6455.

- (77) Mandal, A. K.; Wu, X.; Ferreira, J. S.; Kim, M.; Powell, L. R.; Kwon, H.; Groc, L.; Wang, Y.; Cognet, L. Fluorescent Sp<sup>3</sup> Defect-Tailored Carbon Nanotubes Enable NIR-II Single Particle Imaging in Live Brain Slices at Ultra-Low Excitation Doses. *Sci Rep* **2020**, *10*, 5286.
- (78) Giraldo, J. P.; Wu, H.; Newkirk, G. M.; Kruss, S. Nanobiotechnology Approaches for Engineering Smart Plant Sensors. *Nat Nanotechnol* **2019**, *14*, 541–553.
- (79) Nißler, R.; Bader, O.; Dohmen, M.; Walter, S. G.; Noll, C.; Selvaggio, G.; Groß, U.; Kruss, S. Remote near Infrared Identification of Pathogens with Multiplexed Nanosensors. *Nat Commun* **2020**, *11*, 5995.
- (80) Ackermann, J.; Reger, E.; Jung, S.; Mohr, J.; Herbertz, S.; Seidl, K.; Kruss, S. Smart Slides for Optical Monitoring of Cellular Processes. *Adv Funct Mater* **2023**.

## Table of Contents (TOC)

### Phenyl boronic acid quantum defect

